

Accuracy Analysis of Point Cloud Modeling for Evaluating Concrete Specimens

Nicolas D'Amico and Tzuyang Yu
Department of Civil and Environmental Engineering
University of Massachusetts Lowell
One University Avenue, Lowell, MA 01854, U.S.A.

ABSTRACT

Photogrammetric methods such as structure from motion (SFM) have the capability to acquire accurate information about geometric features, surface cracks, and mechanical properties of specimens and structures in civil engineering. Conventional approaches to verify the accuracy in photogrammetric models usually require the use of other optical techniques such as LiDAR. In this paper, geometric accuracy of photogrammetric modeling is investigated by studying the effects of number of photos, radius of curvature, and point cloud density (PCD) on estimated lengths, areas, volumes, and different stress states of concrete cylinders and panels. Four plain concrete cylinders and two plain mortar panels were used for the study. A commercially available mobile phone camera was used in collecting all photographs. Agisoft PhotoScan software was applied in photogrammetric modeling of all concrete specimens. From our results, it was found that the increase of number of photos does not necessarily improve the geometric accuracy of point cloud models (PCM). It was also found that the effect of radius of curvature is not significant when compared with the ones of number of photos and PCD. A PCD threshold of 15.7194 pts/cm³ is proposed to construct reliable and accurate PCM for condition assessment. At this PCD threshold, all errors for estimating lengths, areas, and volumes were less than 5%. Finally, from the study of mechanical property of a plain concrete cylinder, we have found that the increase of stress level inside the concrete cylinder can be captured by the increase of radial strain in its PCM.

1. INTRODUCTION

Civil engineers have an exclusive responsibility to maintain the safety of civil infrastructure by inspecting and monitoring existing and aged infrastructure systems for necessary maintenance (inspection and repair/rebuild). It is of utmost importance that researchers pursue and develop effective and efficient nondestructive evaluation (NDE) methods. To be effective, the techniques must be easy to use and accurate. To be efficient the techniques must be inexpensive and fast in data collection. Recent advances in pattern recognition and optics have enabled digital photogrammetry to be applied in science and engineering applications. Photogrammetric techniques employ the capabilities of photoscanning algorithms which calculate fiducial key points to effectively calculate the disparities within the triangulations of two dimensional (2D) photographs and to construct a three dimensional (3D) point cloud models (PCM).¹ Such capabilities can be integrated with other conventional NDE methods for condition assessment of civil infrastructure. Combination of photogrammetry and a versatile/mobile platform such as unmanned airborne vehicles (UAV) can further accelerate the process of data collection and reduce inspection costs. Existing photogrammetric techniques include structure from motion (SFM), digital image correlation (DIC), and image mosaicking (IM). Structure from motion (SFM) or dense structure from motion (DSFM) constructs a "naive" geometric model in the form of a PCM by calculating disparities in perspective geometries. Digital image correlation (DIC) uses a pattern of fiducial markings to measure differences in strain over time. DIC requires a multitude of fiducial markers to be effective. While DIC has been employed to produce meaningful results, it still has a number of problems within its practical application capabilities.² By requiring a suitable surface pattern for DIC, a significant investment of time is usually involved. Image mosaicking (IM) stitches multiple images together in order to create a larger image.³ In IM models, the mosaicked image (or images) is typically fit to a predetermined geometry of a structure. IM provides visual information, but loses

Further author information: (Send correspondence to T. Yu)
E-mail: tzuyang-yu@UML.EDU, Telephone: 978-934-2288

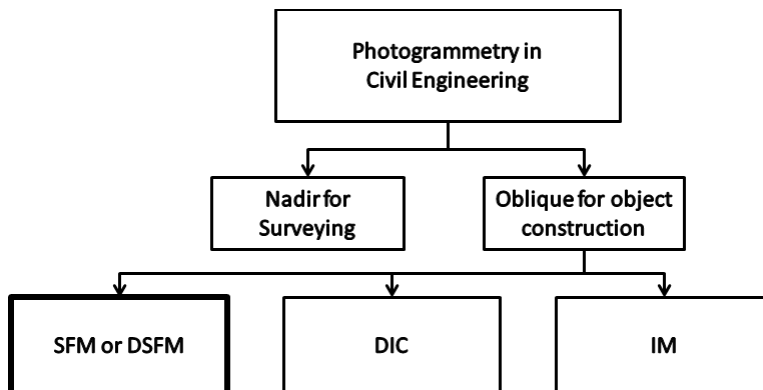


Figure 1. Photogrammetric platforms in civil engineering applications

data about spalling, cracks, surface profiling, and requires a relatively objective approach for condition assessment of structures.⁴ Fig. 1 shows several photogrammetric techniques currently employed in civil engineering applications.

Close-range photogrammetry has significant links with aspects of photographic sciences and computer aided design (CAD) for construction, and architectural concerns.⁵ Accuracy in photogrammetry is strongly associated with distance and size of the object of interest. Unlike DIC methods SFM techniques do not require the use of additional fiducial markers in high quantities. Part of the reason for the success of SFM techniques in civil applications is concrete has a good natural texture which allows for keypoints to be automatically identified.⁶ Accuracies in geometric determination of spacial data using this method have found to outperform total station data as well as laser scan point cloud data. SFM can produce PCM of incredibly high precision detail and accuracy, but are subjugated to the possibility of huge errors if the operator is not familiar with the sources of noise, error, and inconsistencies in the analysis of spacial point cloud information.⁷ Studies have shown the capabilities of photogrammetry to produce geometrically accurate information to a difference of 1 micrometer.⁸ These techniques have been used in civil engineering for a wide range of applications. These applications include crack detection, measurements of distortion, and structural deflections.⁹ Unlike PCM produced from LiDAR systems, photogrammetric invariances are easily characterized due to the existence of a texture pattern showing the object visually.

The objective of this paper is to assess, evaluate, and compute the accuracy of PCM for civil engineering applications, using concrete specimens as examples. The close-range (<10m) SFM oblique approach for object detection is used in this paper. Geometric accuracy is studied with respect to number of photos, radius of curvature, and point cloud density (PCD). In this research, a suggested surface crack profiling approach is demonstrated, and a mechanical analysis is preformed using geometric evaluation and iterative closest point (ICP) methods.

2. EXPERIMENTATION

2.1 Specimen description

A total of seven cementitious specimens were designed and manufactured for this research, categorized into two groups (concrete cylinders and mortar panels). Concrete cylinders (CN01, CN02, CN03, and CND01) were cast with Quickrete Type I Portland cement, all-purpose sand, and all-purpose gravel with a water-to-cement ratio (w/c) of 0.5 and a cement:sand:aggregate ratio of 1:2:3. Among these concrete cylinders, CN01 has an additional 0.475 ml of Darex II AEA admixture. Mortar panels (PN01, PND01, and PND02) were cast with Quickrete Type I Portland cement and all-purpose sand. Mixed with w/c ratios between 0.35 and 0.55 and a sand-to-cement ratio of 2.53:1. All cylinders and panels were moist cured for 28 days and air dried before being used for photogrammetric measurements. Table 1 lists all specimens used in this paper. Figs. 2 to 4 also illustrate these specimens.

Table 1. Considered concrete specimens

Specimen	Acronym	Description
Concrete cylinder	CN01	7.5cm x 15cm, intact
Concrete cylinder	CN02	10cm x 20cm, intact
Concrete cylinder	CN03	10cm x 20cm, intact (mechanically loaded)
Concrete cylinder	CND01	10cm x 20cm, damaged
Mortar panel	PN01	30.48cm x 30.48cm x 2.54cm, intact
Mortar panel	PND01	30.48cm x 30.48cm x 2.54cm, damaged
Mortar panel	PND02	30.48cm x 30.48cm x 2.54cm, damaged

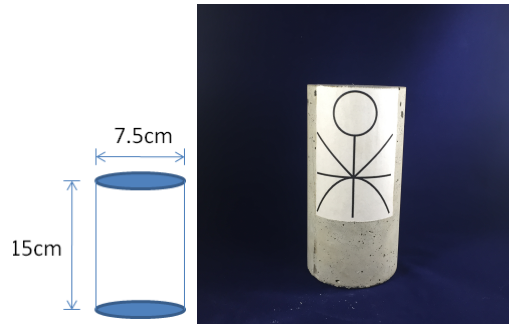


Figure 2. Intact concrete cylinder (CN01); 7.5 cm (diameter) by 15 cm (height)



Figure 3. Concrete cylinders (10 cm (diameter) by 20 cm (height); CN02 (left), CN03 (middle), CND01 (right)

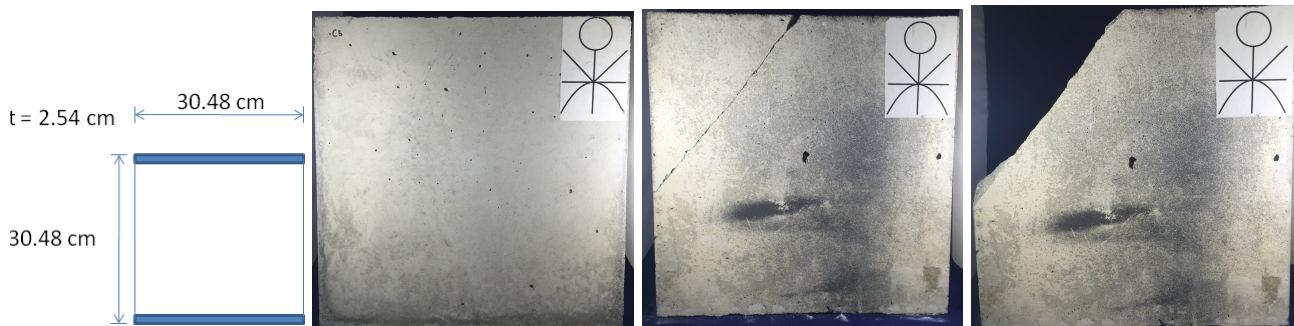


Figure 4. 30.48 cm square panels 2.54 cm thick; (left to right) PN01, PND01, PND02

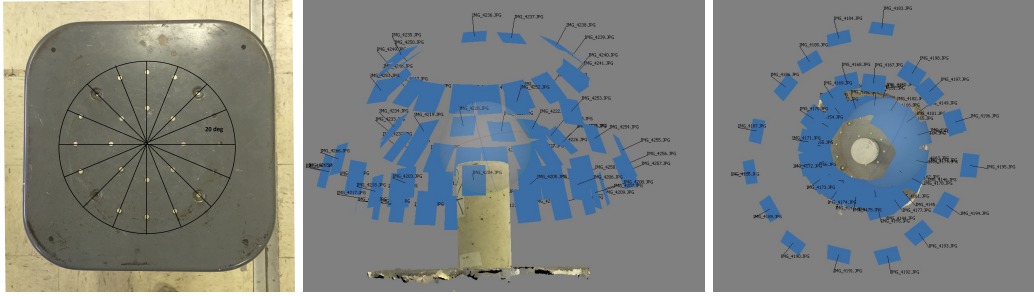


Figure 5. Frame overlap and data acquisition

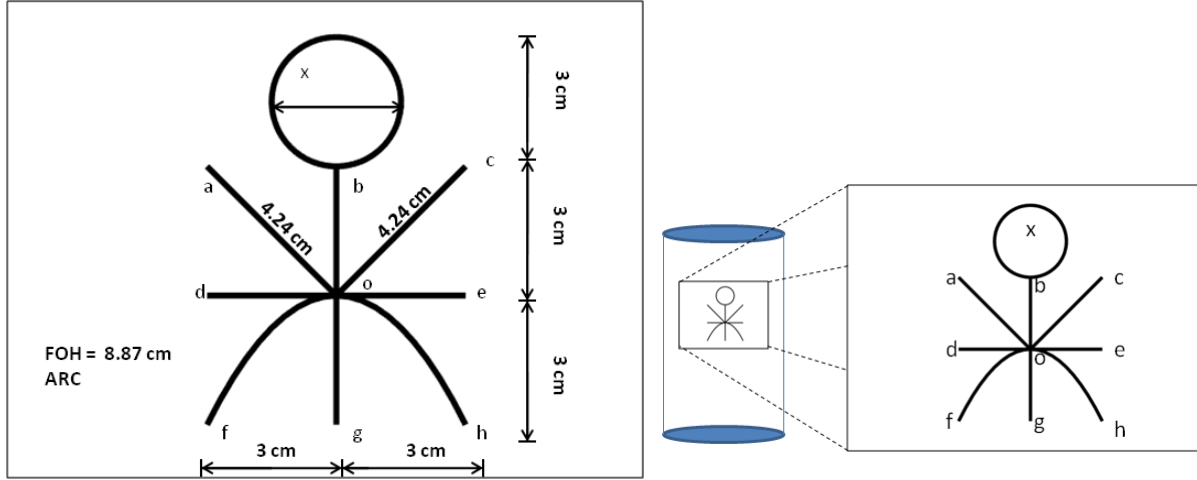


Figure 6. Proposed fiducial marker/calibration marker

2.2 Laboratory setup and data acquisition

In the photogrammetric experimentation of laboratory specimens, all photogrammetric models were constructed out of a maximum of 64 photographs per specimen. These photographs were taken by placing each specimen on a laboratory stool and rotating the specimen for different angles. Four angular regions were defined and sixteen photographs were taken in each region, totaling at sixty-four photographs per specimen. Fig. 5 shows the stool and the data acquisition scheme. In Fig. 5, the blue rectangles indicate the orientation and position of the camera for each photograph.

All photographs were taken in a laboratory with regular room lighting (approximately 175 lux of light intensity) using a smart phone (Iphone 6 by Apple Inc.) with a camera resolution of eight-megapixel and a $1.5\mu\text{m}$ pixel size. A fiducial marker was proposed and used for quantifying the difference (or error) between photogrammetric models and the actual, as shown in Fig. 7. In Fig. 7, the proposed fiducial marker consists of one circle (x), four straight lines ($\bar{o}a, \bar{b}g, \bar{o}c, \bar{d}e$), and one parabola ($\bar{f}oh$). These elements were considered for estimating linear and planar objects on regular and (flat and curved) and irregular (random) surfaces. This fiducial marker was also used as a calibration tool.

In the geometric characterization portion of this study, photogrammetric models were scaled to the smallest width of a known size on each of the specimens, respectively. Scale factor of a model was determined simply by knowing the actual distance between two input points in the model.¹⁰ The fiducial marker was then scaled using manually plotted points. These plotted points were extracted and used to calculate lengths as well as the area of circle (x) seen in Fig. 7. For each length and the circular area (x), a cumulative error was calculated. These results were recorded and analyzed with respect to the number of photographs, PCD, radius of curvature, and level of damage. The volumes of intact and damaged specimens were calculated and compared. By calculating



Figure 7. Progression of PCM construction; (from left to right) undense point cloud, dense point cloud, wire mesh, and textured model

volumetric differences, the amount of spalled or missing concrete from the specimens was determined.

In order to perform surface crack profiling, all models were re-calibrated using the proposed fiducial to ensure a normalized scale. Damaged PCM of specimens (CND01, PND01, and PND02) then underwent a surface crack profiling to show how the technique may help civil engineers evaluate the aging of specimens (and consequently structures). Finally, specimen CN03 underwent a mechanical loading study in which the specimen was uniaxially modeled at 0%, 20% and 40% of its estimated maximum compressive strength using an Instron mechanical testing system (Fig. 16), in accordance with ASTM C469M-14 "Standard Test Method for Static Modulus of Elasticity and Poisson's Ratio of Concrete in Compression".

3. APPROACH

3.1 Image processing

In processing raw photographs for photogrammetric modeling, extra care must be taken to avoid unrealistic portrayal of the target. Physical (optical) errors can occur in the data collection stage, including dirty lenses, unfocused photographs, motion-induced blur, and lack of sufficient amount of photographs. Numerical errors can occur in the image processing stage, including improper photo stitching (or insufficient frame overlap) and inconsistent image resolution (or poor image resolution). In addition, the accuracy of photogrammetric modeling also depends on the area covered by one pixel; the closer the data is acquired the higher the model accuracy.¹¹

In the data processing of this research, the PCM were first triangulated and captured as a normal or undense point cloud. It was then reprocessed as a dense point cloud using a commercially available interpolation algorithm (by Agisoft). The progression of PCM construction is shown in Fig. 6, using specimen CN02 as an example. Upon completion of constructing PCM, they were exported to 3D object files (.OBJ format) in order to be sized and re-sampled for further processing.

3.2 Geometric characterization

For geometric characterization using photogrammetry, length estimation (a straight line, a parabola, a circle), curvature estimation, area estimation, and volume estimation were applied in this research. Number of photos and PCD (or P) were used in quantifying the difference among various PCM. For length estimation, performance of various PCM was evaluated by

$$Er_L(\%) = \frac{1}{m} \sum_i^n \left(\frac{L_{PCM} - L_{act}}{L_{act}} \times 100\% \right)_i \quad (1)$$

where $Er_L(\%)$ = average error in length estimation (%), m = number of data points, L_{PCM} = estimated length using PCM, L_{act} = actual length measured by the fiducial marker. For curvature estimation, radius of curvature (ρ) was used and defined by

$$\rho = \frac{\left[1 + \left(\frac{dy}{dx}\right)^2\right]^{3/2}}{\left(\frac{d^2y}{dx}\right)} \quad (2)$$

The performance of curvature estimation was determined by

$$Er_\rho(\%) = \frac{1}{m} \sum_i^m \left(\frac{\rho_{PCM} - \rho_{act}}{\rho_{act}} \times 100\% \right)_i \quad (3)$$

where $Er_\rho(\%)$ = average error in length estimation (%), m = number of data points, L_{PCM} = estimated length using PCM, L_{act} = actual length measured by the fiducial marker.

For area estimation,

$$Er_A(\%) = \frac{1}{m} \sum_i^m \left(\frac{A_{PCM} - A_{act}}{A_{act}} \times 100\% \right)_i \quad (4)$$

where $Er_A(\%)$ = average error (%), A_{PCM} = estimated area using PCM, A_{act} = actual area measured by the fiducial marker. For volume estimation, the volumes of CN01, CND01, PND01, and PND02 were calculated photogrammetrically as well as by Archimedes displacement principle. The specimens were all submerged into a full water container of known volume and mass. The amount of displaced water was used to estimate volumes physically. Volumes calculated by water displacement were then compared to the volumes calculated by the PCM. Errors in volume estimation were computed by

$$Er_V(\%) = \frac{V_{PCM} - V_{act}}{V_{act}} \times 100\% \quad (5)$$

where $Er_V(\%)$ = error in volume estimation (%), V_{PCM} = estimated volume using PCM, V_{act} = actual volume measured by water displacement.

3.3 Surface crack profiling

The practical advantage to constructing a geometrically accurate photogrammetric model of a specimen or structure is the ability to conduct an optical or visual inspection at anytime. In this experiment, PCM were used to conduct surface crack profiling. The technique shown here exemplifies how these models can be used to easily identify, process, extract, and evaluate surface crack information which enables civil engineers to estimate material strength (or structural stiffness) reduction.

All estimated crack lengths (L_{PCM}) were calculated by the sum of the distances between each line using a raw data imported into a Matlab code, using Eq.(6).

$$L_{PCM} = \sum_{i=2}^n \sqrt{[(x_i - x_{i-1})^2 + (y_i - y_{i-1})^2 + (z_i - z_{i-1})^2]} \quad (6)$$

where L_{PCM} = estimated crack length using selected points, (x_i, y_i, z_i) = Cartesian coordinates of the i -th point, and $(x_{i+1}, y_{i+1}, z_{i+1})$ = Cartesian coordinates of the $(i + 1)$ -th point.

3.4 Mechanical property

Mechanical property (strain components) of concrete was investigated by subjecting a plain concrete cylinder to a compression test using an Instron Material Testing System in the Department of Civil and Environmental Engineering at UMass Lowell (Figure 16). Once the cylinder was loaded, photographs of the cylinder were taken at various aspect angles for photogrammetric modeling. The concrete cylinder was modeled at 0%(unloaded), 20% and 40% of its ultimate load (estimated to be 3,750 psi). The 20% and 40% loads were approximated at 750 lb (3,336 N), and 1,500 lb (6,672 N).

Average surface strain components (ϵ_r , ϵ_θ , ϵ_z) at the midsection of the cylinder were calculated from axial/longitudinal deformation ΔL circumference length s , and cross sectional area A from PCM.

$$\epsilon_z = \frac{\Delta L}{L_0} = \frac{L_i - L_0}{L_0} \quad (7)$$

$$\epsilon_\theta = \frac{\Delta s}{s_0} = \frac{s_i - s_0}{s_0} \quad (8)$$

$$\epsilon_r = \frac{\sqrt{A_i} - \sqrt{A_0}}{\sqrt{A_0}} \quad (9)$$

$$(10)$$

where subscript 0 indicates the unloaded state of the cylinder and subscript i the loaded state of the cylinder. Diameter of the cylinder was also calculated by

$$d = 2\sqrt{\frac{A}{\pi}} \quad (11)$$

where d = diameter (cm) and A = cross sectional area (cm²).

3.5 Comparison with ICP

Performance of PCM was also assessed by comparing with ICP method that compares one PCM with another. ICP has been verified in literature for point cloud stitching using robotic kinematic information to estimate error on a relatively small surface in a lab setting¹² As well as for mapping using a robotic 3D mapper¹³ Even in civil applications to stitch models together to test photogrammetric capabilities as a deflection, or strain gauge measurement system.¹⁴

PCM of unloaded (0%) specimen CN03 was used as the reference for all ICP comparisons. A maximum distance of 0.67872399 cm was used to represent the range of consideration from the reference PCM to other PCM. The ICP algorithm iteratively processed each point on the reference PCM and calculates the distance and number of points within this range. The 20% loaded PCM and 40% loaded PCM were each aligned manually (roughly) and then automatically (finely) to the unloaded, reference PCM. Once alignment was completed, each of the loaded PCM was evaluated for point clouds to determine distances (within a maximum distance of 0.6782399 cm) from the unloaded PCM. A Gaussian distribution function was applied for modeling the distribution of these distances.

4. RESULTS AND ANALYSIS

4.1 Geometric characterization

Six PCM were rendered with different amounts of photographs (64, 32, 22, and 17) and subsequently evaluated for their error with respect to multiple factors (specimen CN03 was not considered in this section as it was used instead for mechanical load testing and was not given a fiducial marker). The results showed that external factors such as frame overlap, possible noise, and surface features, affect the general outcome of the PCM more significantly than the amount of photographs taken.

Figure 8 shows the average error in length estimation (Er_L) as a function of number of photographs (n). In Figure 8, it was observed that average error in length estimation generally decreases with the increase of the

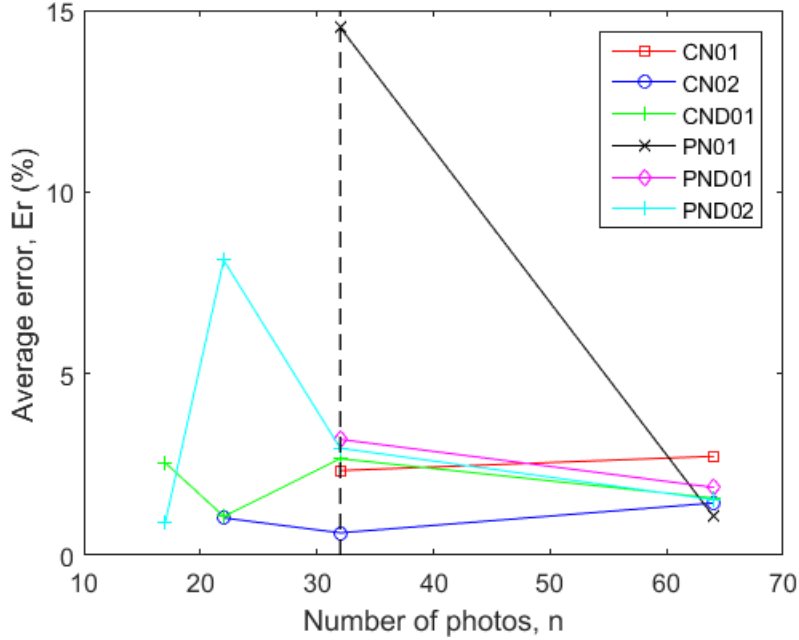


Figure 8. Average error Er_L with respect to photographs taken n

number of photographs. However, average error becomes large when the surface of target lacks of geometric feature (e.g., specimen PN01). On the other hand, should the data points from specimen PN01 in Figure 8 be considered as an outlier, less than 3% of average error can be achieved in surface length estimation. In any case, $n = 32$ photographs can be used as a lower bound for length estimation in this research.

From these results, it was noted that the number of photographs is not the primary factor affecting the performance of PCM and should not be used as the only parameter for assessing the performance (or accuracy) of PCM. Rather, other parameters such as PCD should also be considered as well. Average error in length estimation (Er_L) as a function of PCD (p) was investigated for all the specimens, as shown in Figure 9. In Figure 9, it was found that the average error reduces when PCD increases. A threshold PCD $p = 15.7194$ pts/cm³ was proposed, corresponding to a 2.73% average error in length estimation in this study.

The average error (Er_L) with respect to PCD was modelled by Eq. (12) with an exponential function.

$$Er_L(p) = 11.62e^{-0.1287p} \quad (12)$$

where Er_L = average error in length estimation (%) and p = the PCD of a given model (pts/cm³). The stark difference in the accuracy declines exponentially with an increase in PCD as shown in Figure 10. Although the R^2 of Eq. (12) was as low as 0.5086, this correlation served to conceptualize the importance of PCD in all our PCM cases without any outliers. Therefore, PCD can be used for conducting an accurate account of reliability in photogrammetric modeling.

It was also found that damaged specimens were shown to exhibit less average error than intact specimens regardless of the geometry (Figure 11). Only damaged specimens were able to be rendered and evaluated with as few as 17 photographs. This finding suggests that SFM PCM will be much more easily rendered for damaged structures and specimens than for intact structures and specimens. The effect of radius of curvature (ρ) of specimens was investigated, as shown in Figure 12. Average error was plotted with respect to inverse radius of curvature ($\frac{1}{\rho}$). These results showed that the effect of curvature is in fact not significant enough to outweigh other factors which determine the accuracy of PCM. It was also observed that, although it seems conducive to

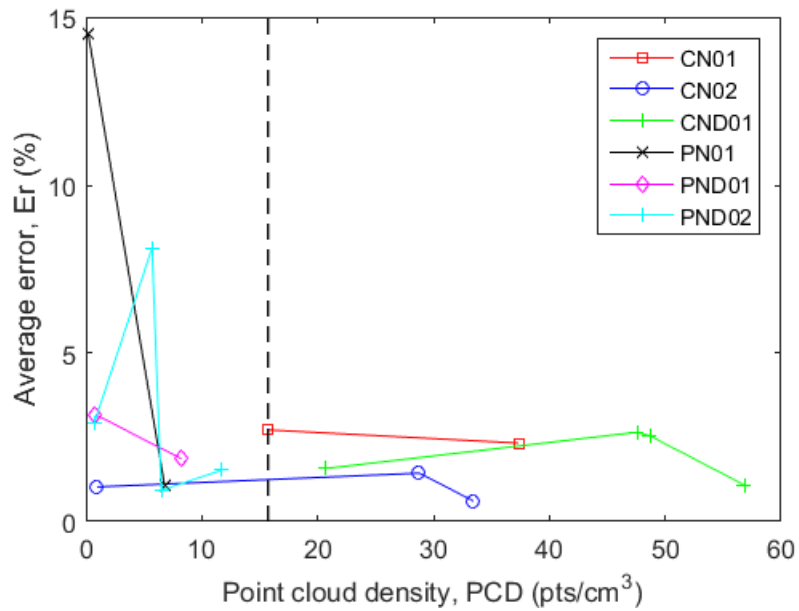


Figure 9. Average error Er_L with respect to PCD p

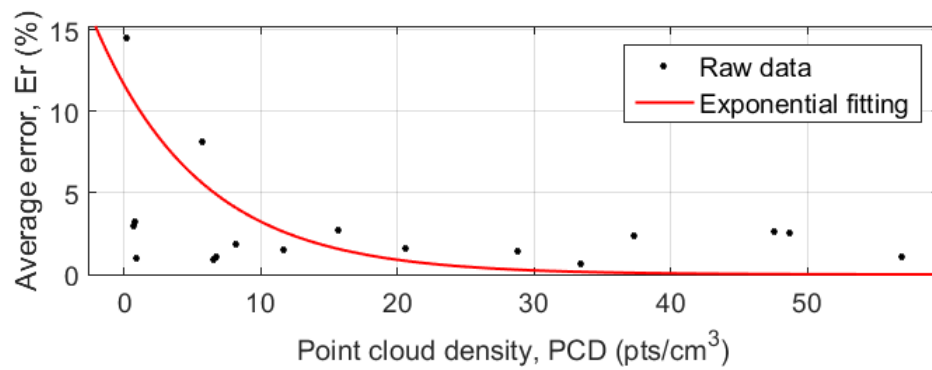


Figure 10. Average error Er_L with respect to PCD – Curve fitting

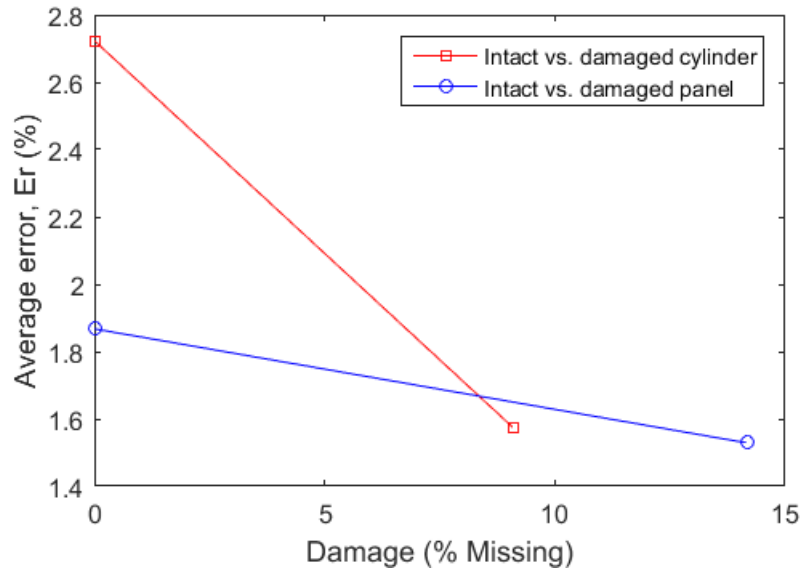


Figure 11. Average error in length estimation – Damaged vs. intact

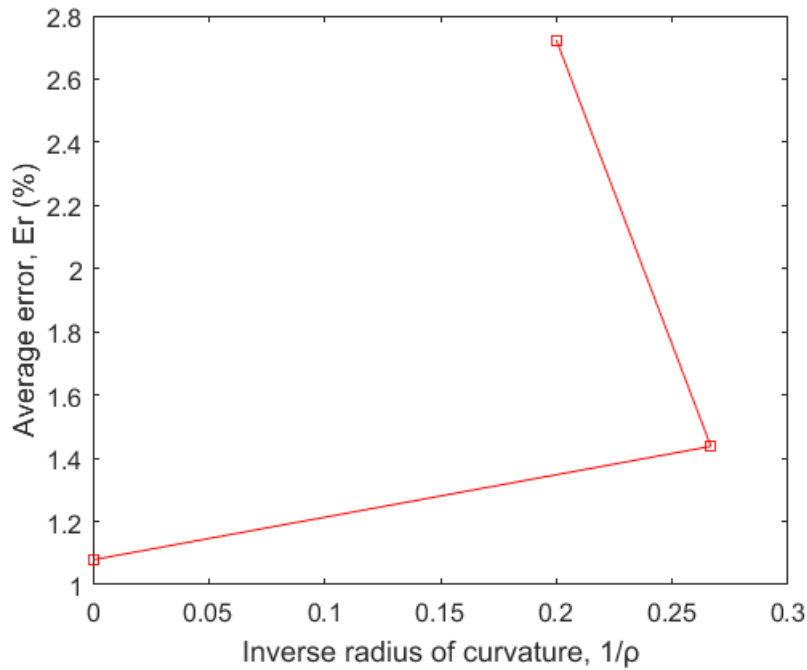


Figure 12. Average error with respect to inverse radius of curvature

compensate for curvature, further research should be carried out on other factors (e.g., surface texture, color contrast, light intensity).

Regarding the performance of PCM on volume estimation, the level of error associated with the volume calculation of each of the considered models was calculated and illustrated in Table 2. All errors remained under 5%, suggesting that the volumes of PCM can be estimated with a reasonable accuracy.

Table 2. Volume calculations and errors

	PCM (cm ³)	Water Displacement (cm ³)	Error (%)
CN01	1525.035	1570.00	2.864013
CND01	1436.947	1369.848	4.898281
PND01	2474	2380	3.94958
PND02	2124.0222	2150	1.208269

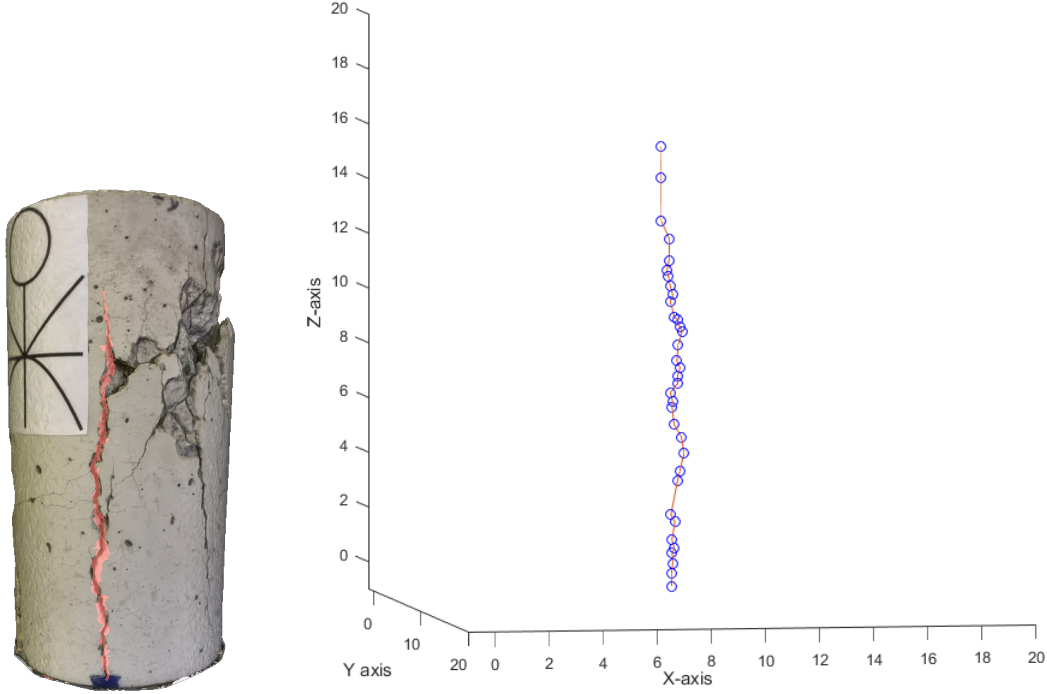


Figure 13. Cylinder CND01 crack 1 identification and extracted crack coordinates (cm)

Four elevations (4 cm, 8 cm, 12 cm, and 16 cm) were chosen on specimen CN03 for estimating cross sectional area, as shown in Table 4 and illustrated in Figure 4.3. It was observed that cross sectional areas increase upon an increasing longitudinal load, due to the Poisson's effect.

Circumference lengths were also directly extracted from the PCM, as shown in Table 5 and illustrated in Figure 4.3.

4.2 Surface crack profiling and damage assessment

Damaged concrete cylinder CND01 and damaged concrete panel PND01 were used in the surface crack profiling using PCM.

Three cracks on specimen CND01 and one crack on specimen PND01 were selected for surface profiling by extracting coordinates of these surface cracks. Three surface cracks on specimen CND01 were reconstructed in a 3D Cartesian coordinate system, as shown in Figures 13 and 14. One surface crack on specimen PND01 was also reconstructed in a 3D Cartesian coordinate system, as shown in Figure 15. Average crack lengths and widths were calculated from the PCM of specimens CND01 and PND01, as shown in Table 3. Figures 13-15 exemplify how the surface cracks can be profiled, extracted and evaluated. The demonstrated ability of PCM to extract information of surface cracking proves their viability for automated visual inspection.

4.3 Mechanical property

In the PCM application for mechanical property, strain components were calculated from the 3D PCM of specimens. Radial strains (ϵ_r) were estimated from PCM at 20% and 40% loading levels, as shown in Figure

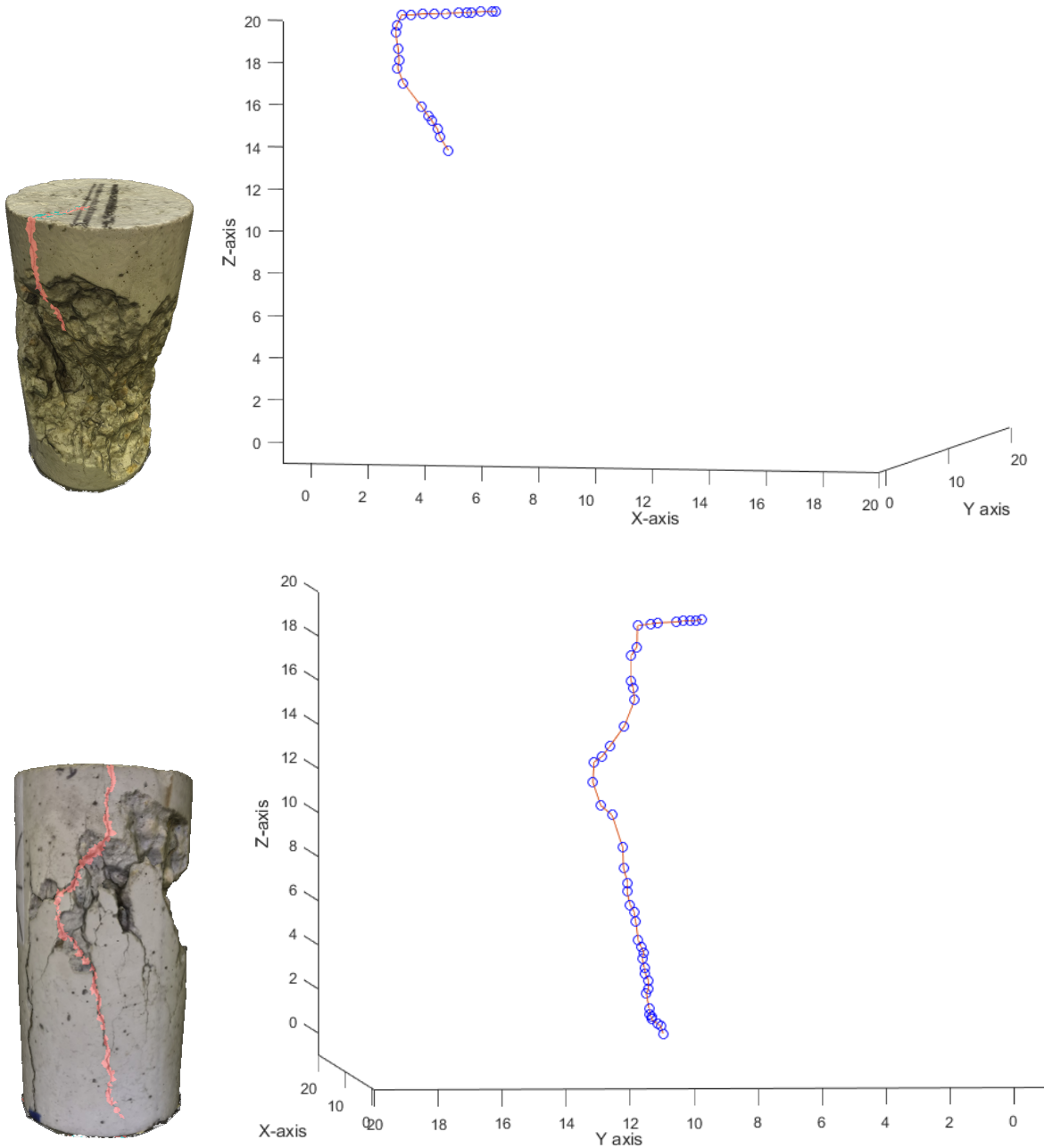


Figure 14. Cylinder CND01 cracks 2 and 3 identification and extracted crack coordinates (Unit: cm)

Table 3. Crack length and width estimations of specimens CND01 and PND01 (Unit: cm)

	Total length	Avg length	Avg width
CND01-64	21.3694	7.123133	0.114904
PND01-64	52.8676	52.8676	0.02533

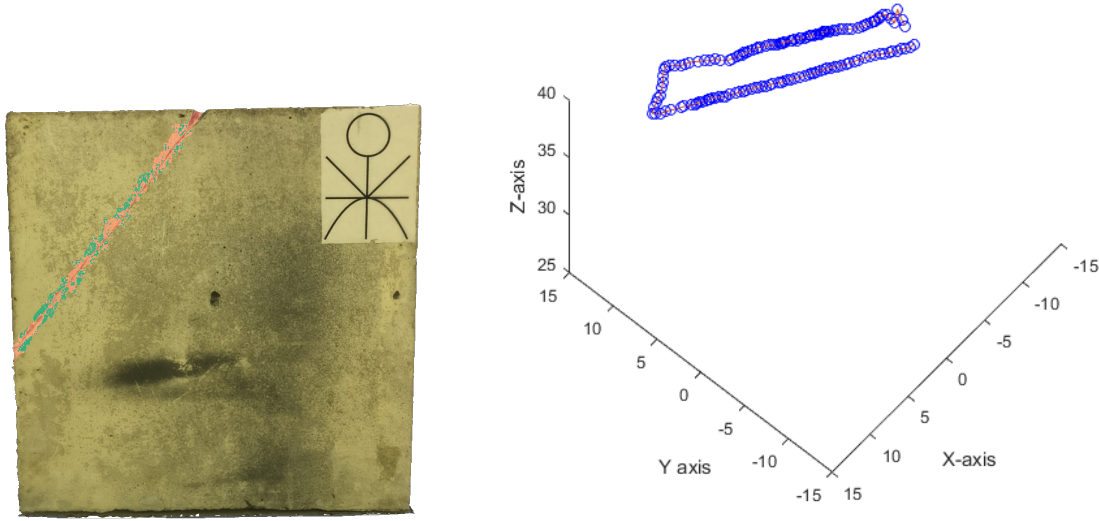


Figure 15. Panel PND01 crack identification and extracted crack coordinates (Unit: cm)

Table 4. Cross sectional areas A_s at 0%, 20%, and 40% loading levels

	0% (cm^2)	20% (cm^2)	ΔA_s (%)	40% (cm^2)	ΔA_s (%)
Z4	82.409714	82.84245	0.525097	84.17691	2.144403
Z8	83.3246	83.97095	0.775698	85.2244	2.279994
Z12	84.149651	84.94586	0.946185	86.08547	2.300448
Z16	85.00502	85.86791	1.015107	86.75012	2.05294
Avg	83.722246	84.40679	0.817638	85.55922	2.194134

4.3. Angular strains (ϵ_θ) were computed from PCM at 20% and 40% loading levels, as shown in Figure 4.3. Longitudinal strains (ϵ_z) were calculated from PCM 20% and 40% loading levels, as shown in Table 6.

4.4 Comparison with ICP

The Gaussian distributions from the 20% and 40% loading levels ICP models were determined, as shown in Figures 21 and 22, respectively. It was observed that the mean distance of 20% loaded ICP model is less than the one of 40% loaded ICP model, while their standard deviations were not too different from each other. Mean distance of the 40% loaded ICP model was almost twice the amount of the 20% loaded ICP model. It was found that the increase in average iterative point distances provides information correlated to the relative loading level of the specimen.

Table 5. Circumference values s at 0%, 20%, and 40% loading levels (cm)

	0%	20%	40%
Z4	32.3490	31.8448	32.6327
Z8	32.5192	32.4950	32.7106
Z12	32.3389	32.1098	32.8556
Z16	32.7118	32.4592	32.8102
Avg	32.47973	32.2272	32.75228

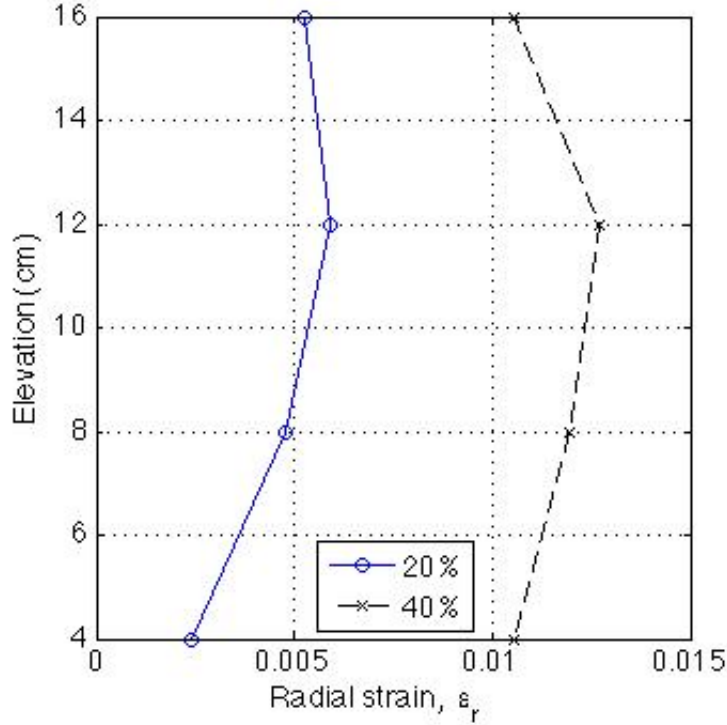


Figure 16. Radial strain ϵ_r at 20% and 40% loading levels

Table 6. Estimated diameters and longitudinal strains at 20% and 40% loading using average diameter from surface area calculations

	0%	20%	40%
Diameter (d)(cm)	10.324654	10.36678	10.43731
Longitudinal strain (ϵ_z)	NaN	0.00408	0.010911

5. CONCLUSION

This paper reports our analysis on the accuracy of point cloud models for condition assessment using concrete cylinders and panels. Photogrammetric point cloud models can be evaluated for accuracy using the number of photographs and point cloud density (PCD), although the number of photographs does not guarantee the construction of accurate point cloud models. Once calibrated, photogrammetric models can provide information such as surface crack profiles with lengths and widths estimated. PCM can provide a cross sectional analysis which allows civil engineers to identify critical cross sections in concrete structures. Mechanical strains can be estimated from PCM for structural health monitoring.

Major findings from this research are concluded in the following.

- **Geometric characterizations**

- Effect of number of photographs – From our research on concrete cylinders and panels, it was found that the number of photographs (n) does not necessarily guarantee the accuracy of PCM for condition assessment. In other words, the number of photographs should not be used as the only parameter to assess the accuracy of PCM. Our experimental work on laboratory specimens also suggests that, $n = 32$ photographs can be used as a lower bound for length estimation with less than a 5% average error.
- Effect of point cloud density (PCD or p) – PCD can be used in general as a way to understand and determine the accuracy of photogrammetric PCM. Due to the nature of photogrammetric modeling,

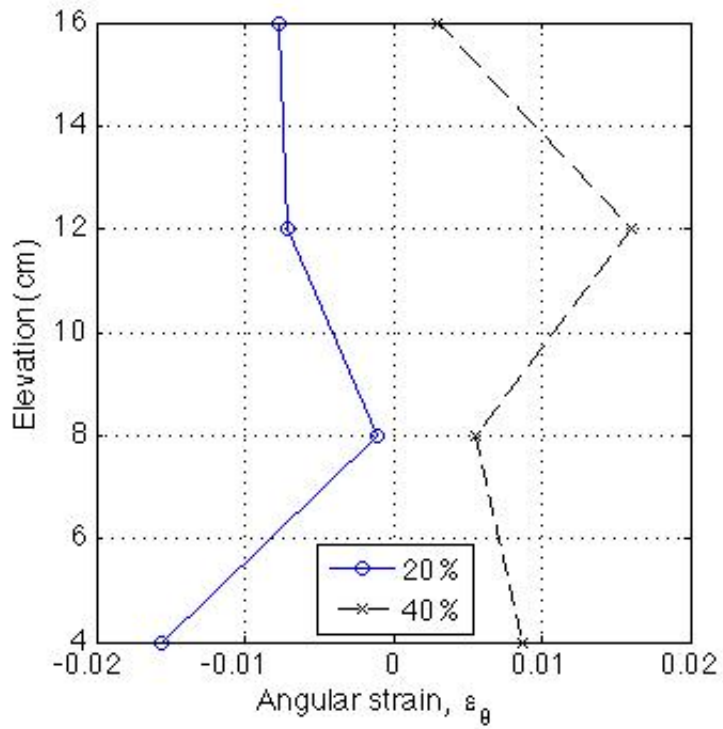


Figure 17. Angular strain ϵ_θ at 20% and 40% loading levels

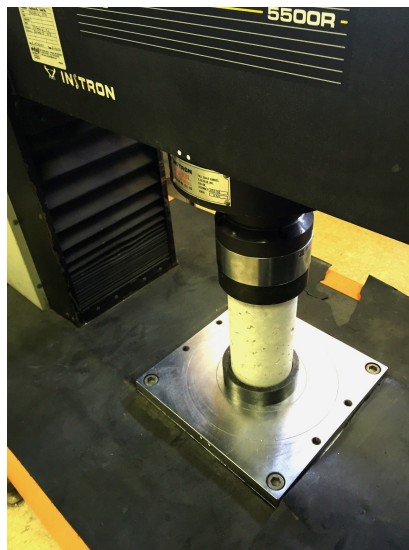


Figure 18. Instron material testing system

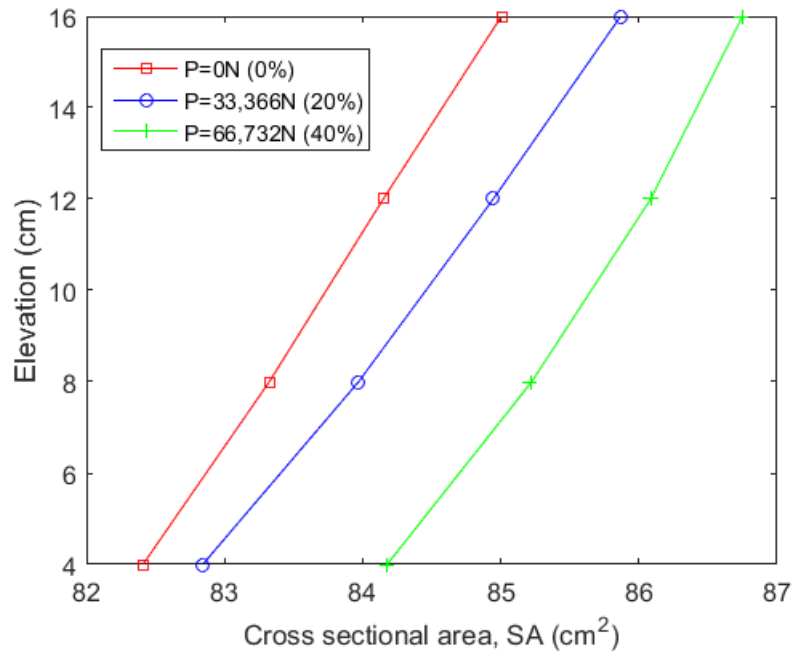


Figure 19. Cross sectional areas at four elevations on specimen CN03

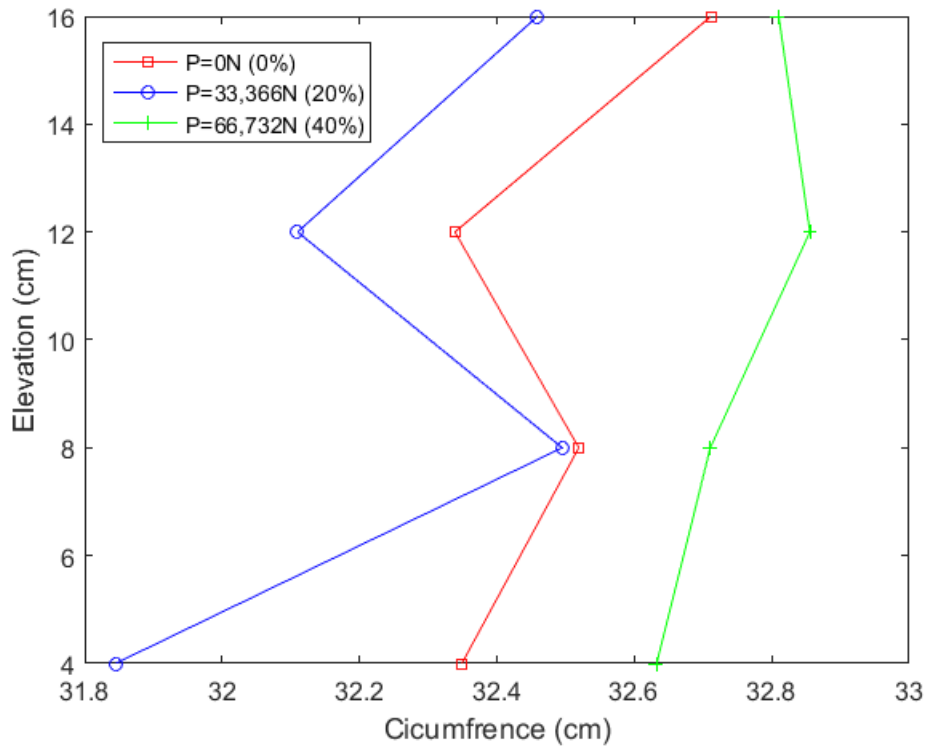


Figure 20. Circumference s at four elevations on specimen CN03

Gauss: mean = -0.032790 / std.dev. = 0.046743 [54 classes]

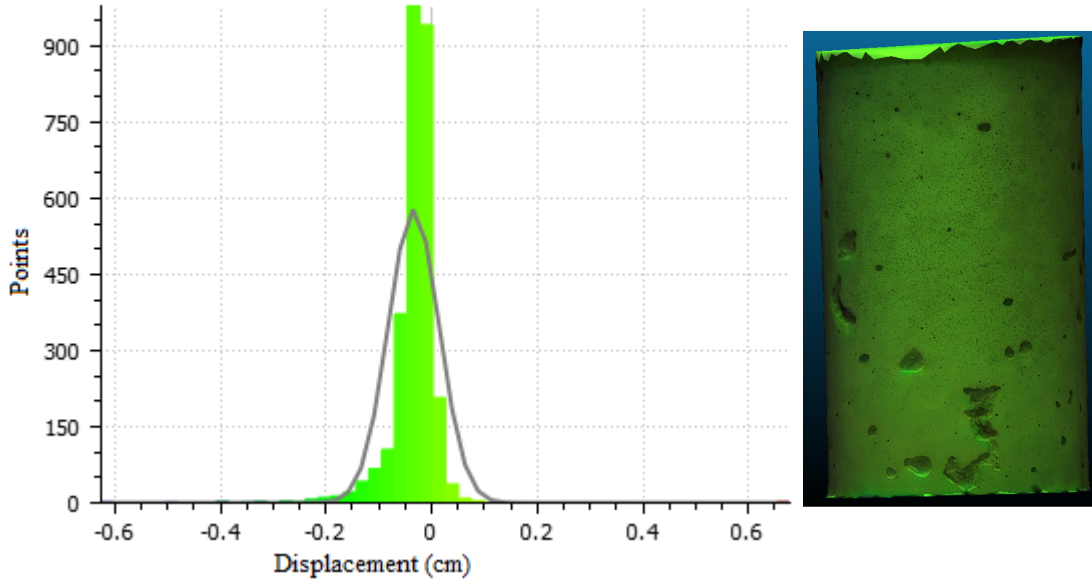


Figure 21. ICP result for 20% loading level

Gauss: mean = -0.071393 / std.dev. = 0.048468 [49 classes]

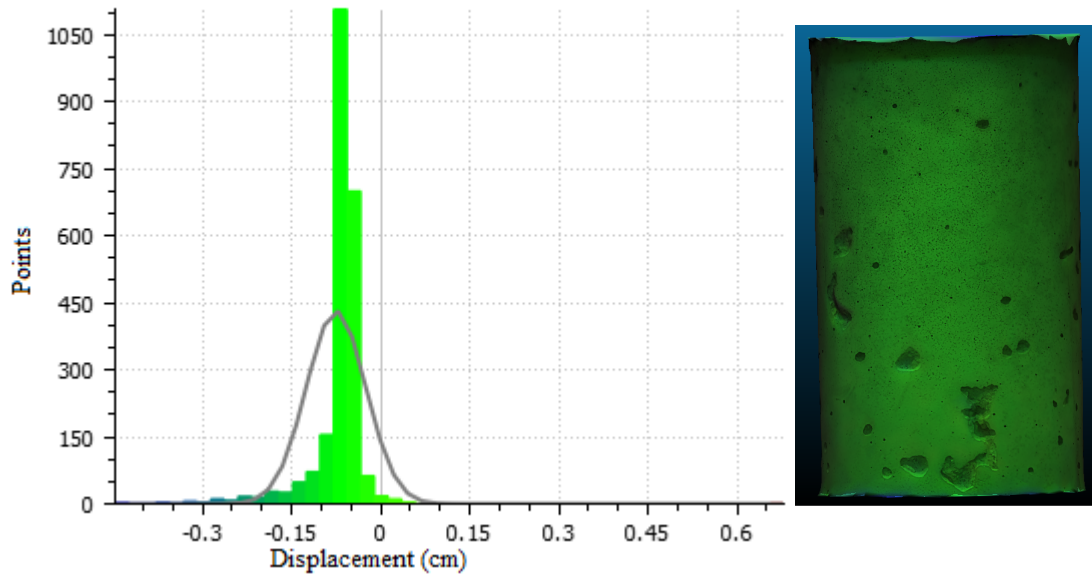


Figure 22. ICP result for 40% loading level

it is imperative that a PCD threshold is established which defines a relative accuracy in the modeling. In our research, a lower bound of PCD $p = 15.7194 \text{ pts/cm}^3$ can be used to ensure the accuracy of PCM with a 2.73% average error. An exponential function is also proposed to model this relation (Eq. (12)).

- Surface feature of concrete specimens – Damaged specimens are more easily to be modelled than intact specimens since the presence of cracks or anomalies represents more surface features with damaged specimens. In other words, SFM PCM will be much more easily rendered for damaged structures as for intact structures, suggesting the promising potential for field applications.
 - Effect of surface curvature – From our experimental result on laboratory concrete cylinders and panels, average error does not demonstrate a clear pattern with surface curvature (quantified by radius of curvature).
 - Volume estimation using PCM – By using PCM, estimation error can be less than 5% in our results.
 - In this study after thorough compilation of results, the overall errors remained below 5% for lengths, areas, and even volumes of concrete specimens when $\text{PCD} > 15.7194 \text{ pts/cm}^3$. While not entirely consistent, these results have demonstrated that photogrammetric reliability is in fact within a reasonable and acceptable range for concrete specimens (and potentially structures).
 - Comparison with ICP – The increase in average iterative point distances in ICP models provides information correlated to the relative loading level of the specimen. The average distance differences in each loaded specimen as compared to the unloaded one can be used as an indicator to the strain (or loading) level of specimens or structures.
- **Surface crack profiling**
The feasibility of using PCM for surface crack profiling is demonstrated in this research. Photogrammetric models can be used to estimate crack lengths and widths on concrete surface.
 - **Mechanical property**
 - The increase in average iterative point distances provides data which can be correlated to the relative loading level of the specimen.
 - Longitudinal and angular strain – With the use of reference markers (e.g., fiducial marker in this research), longitudinal and angular strains can be calculated from circumference data in PCM.
 - Radial strain – For circular targets from which photographs can be taken from all angles, radial strains can be calculated from estimated cross sectional areas in PCM.

In conclusion, structure from motion (SFM) photogrammetric modeling of concrete specimens (and structures) provides promising results as a tool for condition assessment and damage detection. As the imminence of structural deficiency becomes more apparent, new, practical, and cost efficient techniques are needed for civil engineers to evaluate the strength and material properties of concrete structures. The analysis presented in this paper demonstrates the capabilities of photogrammetric modeling for future concrete health assessment.

6. ACKNOWLEDGMENT

This work was partially supported through a grant (OASRTRS-14-H-UML) from the Office of the Assistant Secretary for Research and Technology (OST-R) of the U.S. Department of Transportation (DOT)(Program manager: Caesar Singh). The authors also appreciate the assistance from Massachusetts Department of Transportation (MassDOT) and the City of Lowell (MA).

7. DISCLAIMER

The views, opinions, findings and conclusions reflected in this presentation are the responsibility of the authors only and do not represent the official policy or position of the USDOT/OST-R or any State or other entity.

REFERENCES

1. Goshtasby, A. A., [*2-D AND 3-D Image Registration for medical, remote sensing and industrial applications*], John Wiley and Sons Inc., 111 River Street Hoboken, NJ (2001).
2. MacNish, C., Hassan, G. M., Dyskin, A. V., and Pasternak, E., “Towards affordable and robust remote photogrammetric sensing for early warning of fracturing and structural failure,” in [*Humanitarian Technology Conference (R10-HTC), 2015 IEEE Region 10*], 1–6 (Dec 2015).
3. Chaiyasarn, K., Kim, T.-K., Viola, F., Cipolla, R., and Soga, K., “Distortion-free image mosaicing for tunnel inspection based on robust cylindrical surface estimation through structure from motion,” *Journal of Computing in Civil Engineering* **0**(0), 04015045 (2015).
4. Lattanzi, D. and Miller, G. R., “3d scene reconstruction for robotic bridge inspection,” *Journal of Infrastructure Systems* **21**(2), 04014041 (2015).
5. Thomass Luhmann, Stuart Robson, S. K. J. B., [*Close-Range Photogrammetry and 3D Imaging*], Walter de Gruyter GmbH and Co. KG; Gottingen., 121 High St. Boston, MA, 2nd ed. (2014).
6. Almeida, G., Biscaia, H., Chastre, C., Fonseca, J., and Melcio, F., “Displacement estimation of a rc beam test based on tss algorithm,” in [*Information Systems and Technologies (CISTI), 2010 5th Iberian Conference on*], 1–4 (June 2010).
7. Sapirstein, P., “Accurate measurement with photogrammetry at large sites,” *Journal of Archaeological Science* **66**, 137 – 145 (2016).
8. Mingli, D., Jun, W., Bixi, Y., Xiaoping, L., and Ruibao, C., “Accuracy evaluation method and experiments for photogrammetry based on 3d reference field,” in [*Advanced Technology of Design and Manufacture (ATDM 2010), International Conference on*], 489–492 (Nov 2010).
9. Maas, H.-G. and Hampel, U., “Photogrammetric techniques in civil engineering material testing and structure monitoring,” *Journal of Photogrammetric Engineering and Remote Sensing* (2006).
10. Bemis, S. P., Micklethwaite, S., Turner, D., James, M. R., Akciz, S., Thiele, S. T., and Bangash, H. A., “Ground-based and uav-based photogrammetry: A multi-scale, high-resolution mapping tool for structural geology and paleoseismology,” *Journal of Structural Geology* **69, Part A**, 163 – 178 (2014).
11. Fathi, H. and Brilakis, I., “Automated sparse 3d point cloud generation of infrastructure using its distinctive visual features,” *Advanced Engineering Informatics* **25**(4), 760 – 770 (2011). Special Section: Advances and Challenges in Computing in Civil and Building Engineering.
12. Shi, Q. and Xi, N., “Automated data processing for a rapid 3d surface inspection system,” in [*Robotics and Automation, 2008. ICRA 2008. IEEE International Conference on*], 3939–3944 (May 2008).
13. Bedkowski, J., Peka, M., Majek, K., Fitri, T., and Naruniec, J., “Open source robotic 3d mapping framework with ros2014; robot operating system, pcl2014; point cloud library and cloud compare,” in [*Electrical Engineering and Informatics (ICEEI), 2015 International Conference on*], 644–649 (Aug 2015).
14. Jafari, B., Khaloo, A., and Lattanzi, D., “Long-term monitoring of structures through point cloud analysis,” (2016).